Biogeosciences, 9, 5095–5109, 2012
www.biogeosciences.net/9/5095/2012/
doi:10.5194/bg-9-5095-2012

Biogeosciences

Controlling factors of the oxygen balance in the Arabian Sea's OMZ

L. Resplandy[1], **M. Lévy**[2], **L. Bopp**[1], **V. Echevin**[2], **S. Pous**[3], **V. V. S. S. Sarma**[4], **and D. Kumar**[4]

[1]LSCE – Laboratoire des Sciences du Climat et de l'Environnement (CEA, CNRS, UVSQ), UMR8212, IPSL, France
[2]LOCEAN – Laboratoire d'Océanographie et du Climat: Experimentation et Approches Numériques (CNRS, IRD, UPMC, MNHN), IPSL, France
[3]Museum National d'Histoire Naturelle, Paris, France
[4]National Institute of Oceanography, Goa, India

Correspondence to: L. Resplandy (laure.resplandy@lsce.ipsl.fr)

Received: 30 March 2012 – Published in Biogeosciences Discuss.: 10 May 2012
Revised: 9 October 2012 – Accepted: 13 November 2012 – Published: 13 December 2012

Abstract. The expansion of OMZs (oxygen minimum zones) due to climate change and their possible evolution and impacts on the ecosystems and the atmosphere are still debated, mostly because of the unability of global climate models to adequatly reproduce the processes governing OMZs. In this study, we examine the factors controlling the oxygen budget, i.e. the equilibrium between oxygen sources and sinks in the northern Arabian Sea OMZ using an eddy-resolving biophysical model.

Our model confirms that the biological consumption of oxygen is most intense below the region of highest productivity in the western Arabian Sea. The oxygen drawdown in this region is counterbalanced by the large supply of oxygenated waters originated from the south and advected horizontally by the western boundary current. Although the biological sink and the dynamical sources of oxygen compensate on annual average, we find that the seasonality of the dynamical transport of oxygen is 3 to 5 times larger than the seasonality of the biological sink. In agreement with previous findings, the resulting seasonality of oxygen concentration in the OMZ is relatively weak, with a variability of the order of 15 % of the annual mean oxygen concentration in the oxycline and 5 % elsewhere. This seasonality primarily arises from the vertical displacement of the OMZ forced by the monsoonal reversal of Ekman pumping across the basin. In coastal areas, the oxygen concentration is also modulated seasonally by lateral advection. Along the western coast of the Arabian Sea, the Somali Current transports oxygen-rich waters originated from the south during summer and oxygen-poor waters from the northeast during winter. Along the eastern coast of the Arabian Sea, we find that the main contributor to lateral advection in the OMZ is the Indian coastal undercurrent that advects southern oxygenated waters during summer and northern low-oxygen waters during winter. In this region, our model indicates that oxygen concentrations are modulated seasonally by coastal Kelvin waves and westward-propagating Rossby waves.

Whereas on seasonal time scales the sources and sinks of oxygen are dominated by the mean vertical and lateral advection (Ekman pumping and monsoonal currents), on annual time scales we find that the biological sink is counterbalanced by the supply of oxygen sustained by mesoscale structures (eddies and filaments). Eddy-driven advection hence promotes the vertical supply of oxygen along the western coast of the Arabian Sea and the lateral transport of ventilated waters offshore the coast of Oman and southwest India.

1 Introduction

Oxygen minimum zones (OMZs) are intermediate-depth layers characterized by very low oxygen saturations. Most pronounced OMZs are found in the eastern north and south Pacific Ocean and the northern Arabian Sea, where oxygen concentrations $\leq 20\,\mu mol\,L^{-1}$ are frequently observed between 100 and 1000 m (Paulmier and Ruiz-Pino, 2009; Bianchi et al., 2012). Suboxic conditions in the water column are usually associated with low dynamical oxygen supply and high oxygen demand. OMZs are hence found in regions of low ventilation by subsurface currents and productive upwelling systems, where intense biological uptake of oxygen associated with bacterial respiration and remineralisation occur.

OMZs are carefully examined for their possible interactions with the climate system and impacts on ecosystems. They could modulate atmospheric concentrations of major greenhouse gases such as CO_2 and N_20 (Falkowski, 1997; Naqvi et al., 1998; Codispoti et al., 2001; Naqvi et al., 2006; Lam et al., 2011; Bianchi et al., 2012) and constitute a respiratory barrier influencing the ecosystems structure (Diaz and Rosenberg, 2008; Levin et al., 2009; Stramma et al., 2011). Recent studies based on observations suggest that the volume of OMZs' suboxic waters has increased over the past decades (Stramma et al., 2008) and could expand further in response to ocean warming and increased stratification associated with climate change (Sarmiento et al., 1998; Keeling et al., 2010). However, no consensus seems to arise from coupled model future scenarios, most likely because of the uncertainties on the processes governing the balance between oxygen sources and sinks of OMZs in these global low resolution models (Froelicher et al., 2009; Gnanadesikan et al., 2012; Stramma et al., 2012). Improving our understanding of these sources and sinks of oxygen and their representation in our climate models is therefore of primary importance when considering the future evolution and impacts of OMZs. In this study we focus on the OMZ of the northern Arabian Sea, one of the three major OMZs.

Unlike other OMZs that are located below intense eastern boundary upwelling systems, the OMZ in the Arabian Sea is shifted eastward from the region of highest productivity (Fig. 1d and h) (de Sousa et al., 1996; Morrison et al., 1999). In addition, the oceanic circulation and the biological activity, which are the main sources and sinks of oxygen, are tremendously modulated at seasonal scale by the monsoon system (Fig. 1a–d) and at small spatial scales by mesoscale structures (filaments and eddies, Fig. 3). Despite this considerable spatio–temporal variability in surface ocean dynamics and biological activity, no dramatic seasonal and spatial variability has been observed in oxygen concentrations within the OMZ in the Arabian Sea (Fig. 1g and h) (Morrison et al., 1999), suggesting the existence of a complex and subtle balance between the sources and sinks of oxygen. Numerous hypotheses have been proposed to explain the spatial and seasonal maintenance of the OMZ in the northeastern Arabian Sea, including dynamical and biological mechanisms.

It was first thought that the slow advection of low-oxygen waters into the Arabian Sea's OMZ limited the variations in oxygen levels (Sverdrup et al., 1942). The maintenance of oxygen concentrations at seasonal scales was then attributed to high organic matter decomposition rates consistent with the high levels of local productivity during monsoonal blooms (Ryther and Menzel, 1965). These initial hypotheses, however, were refuted by Olson et al. (1993) who argued that the residence time in the OMZ (~ 10 yr) did not support the slow advection hypothesis and that observations of surface productivity, while high, preclude an exceptional high consumption rate at depth. Later, the transport of oxygenated waters by the western boundary current (Swallow, 1984; Sarma, 2002), mixing by mesoscale eddies (Kim et al., 2001) and strong detrital sinking rates enhancing export to the deep ocean (Wiggert and Murtugudde, 2007), were invoked to explain the presence of relatively high oxygen concentration below the region of highest productivity. The recent process study of McCreary et al. (2012) confirmed the prominent role of oceanic circulation in controlling the spatial distribution of the OMZ in the Arabian Sea. Using sensitivity experiments, they identified the transport of oxygen by the eastern boundary current and eddy mixing as essential processes to reproduce the eastward shift of the OMZ. This result is in line with the prominent role of mesoscale structures (eddies and filaments) on the modulation of dynamical and biological processes identified in the Arabian Sea; numerous observations and modelling studies highlighted the significant impact of mesoscale structures on the transport of water and nutrients along the western boundary and offshore into the Arabian Sea (Flagg and Kim, 1998; Manghnani et al., 1998; Lee et al., 2000; Kim et al., 2001; Kawamiya, 2001; Resplandy et al., 2011), the phytoplankton productivity (Brink et al., 1998; Marra et al., 1998; Resplandy et al., 2011) and the particle flux to the deep ocean (Honjo et al., 1999). Finally, Sarma (2002) suggested that the absence of seasonality in the OMZ resulted from the compensation between the physical ventilation of the OMZ and biological consumption of oxygen during each season. In this view, during the monsoon periods active organic matter remineralisation compensates the large oxygen transport, whilst during intermonsoons the remineralisation of the residual organic matter from the monsoonal blooms is sufficient to compensate the low oxygen transport. This hypothesis could not be verified given the absence of reliable seasonal estimates of oxygen consumption (Sarma, 2002).

In this context, the aim of this paper is to examine the annual sources and sink terms governing the oxygen budget in the Arabian Sea. Given the strong seasonal and spatial variability of biological activity and oceanic circulation, we tackle this issue by examining the seasonal contributions of the various sources and sinks in three key regions of the OMZ before considering their impact on the maintenance of the OMZ on annual time scale. This issue is addressed for the first time with a coupled biophysical model of the northern Indian Ocean that explicitly resolves eddies (Resplandy et al., 2011). The model setting and the method to derive the oxygen budget are presented in Sect. 2. Section 3 describes the spatial distribution and seasonality of oxygen concentrations in the model and observations. Section 4 investigates the drivers of the oxygen seasonality in three key regions and the factors controlling the maintenance of the OMZ using the oxygen budget simulated in the model. Finally, Sect. 5 discusses the main results and gives a synthesis of the physical and biogeochemical factors controlling the OMZ in the Arabian Sea.

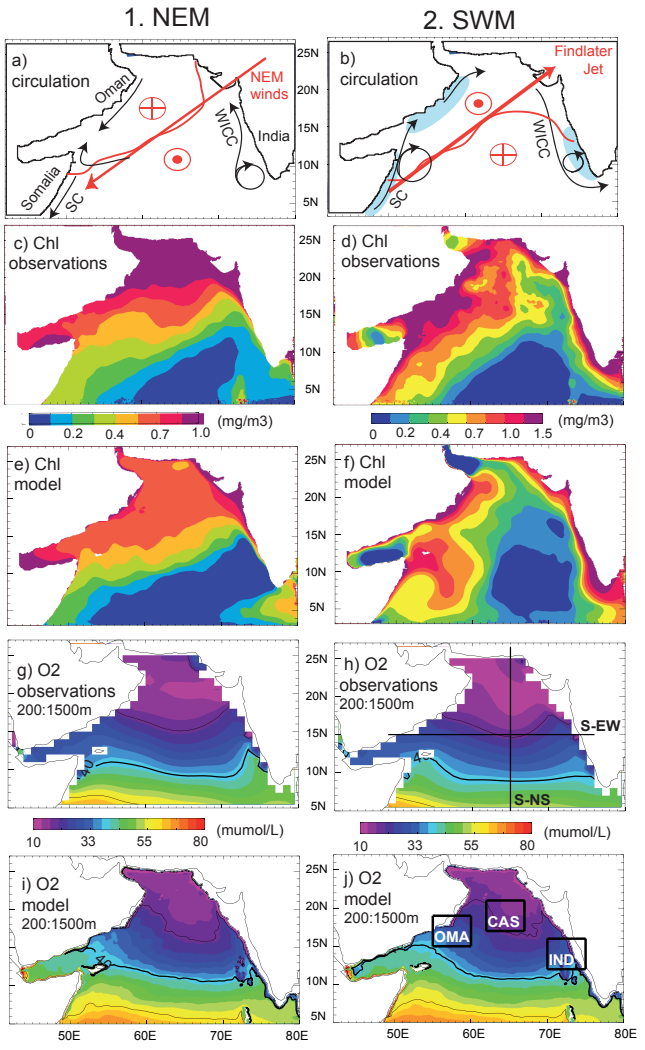

Fig. 1. Climatological maps during the northeast monsoon (NEM, December–February) and southeast monsoon (SWM, June–August): **(a)**, **(b)** Schematic representation of dominant winds (red arrows), oceanic circulation (black arrows), coastal upwelling systems (blue shading) and Ekman pumping (red symbol) adapted from Schott and McCreary (2001). The reversing Somali Current (SC) and Western Indian Coastal Current (WICC) are indicated; **(c–f)** surface chlorophyll (Chl, in mg m^{-3}) climatology from satellite SeaWiFS (1998–2005) **(c)**, **(d)** and simulated in the model **(e)**, **(f)**; **(g–j)** oxygen concentration averaged between 200 and 1500 m in WOA09 **(g)**, **(h)** and simulated in the model **(i)**, **(j)**. Sections EW and NS presented in Figs. 4 and 5 are indicated in **(h)**. Regions CAS, OMA and IND presented in Figs. 6–8 are indicated in **(j)**.

2 Model description

2.1 Physical model

The eddy-resolving model configuration of Resplandy et al. (2011) based on the NEMO OGCM is used (Madec, 2008). The model domain covers the northern Indian Ocean between 5° S and 27° N and includes both the Bay of Bengal and the Arabian Sea. Only results from the Arabian Sea are presented in this study. The horizontal resolution is 1/12° (∼9 km) and the vertical grid has 46 levels increasing from 6 m at the surface to 250 m at depth. Northern, eastern and western boundaries are closed by continental masses. The southern boundary (5° S) is a radiative open boundary (Treguier et al., 2001), constrained with a 150 days time scale relaxation to the monthly meridional velocities, temperature and salinity of the interannual global 1/4° simulation DRAKKAR025-G70 (Barnier et al., 2006). The straits of Bab el Mandeb, Hormuz and Malacca are closed and damped in temperature and salinity toward the Levitus climatology (Levitus et al., 1998) with a 10 days time scale. The initial state is at rest. Temperature and salinity are initialized with the Levitus climatology. The model is forced with the interannual hybrid DRAKKAR Forcing Set 4 (DFS4) extensively described in Brodeau et al. (2009). One of the major challenges is to ensure the model stability in the highly energetic western boundary current and the associated anticyclonic gyre called the Great Whirl, without using excessive momentum dissipation that would damp small-scale processes elsewhere.

Momentum, temperature and salinity are therefore advected using a third-order, diffusive, upstream-biased scheme (Shchepetkin and McWilliams, 2005; Madec, 2008). The intrinsic horizontal diffusivity of this scheme is proportional to the current velocity u ($\frac{1}{12}\Delta x^3|u|$, with Δx the horizontal resolution in m). The resulting dissipation is of the order of 6×10^{10} m^4 s^{-1} in the Great Whirl (where currents reach 1 m s^{-1}) and 2 orders of magnitude lower in the central Arabian Sea (where currents are of the order of 1 cm s^{-1}). This scheme does not require any additional dissipation and diffusivity to ensure numerical stability. Vertical mixing is modelled with a prognostic turbulent kinetic energy scheme, with background vertical diffusion and viscosity of 10^{-5} m^2 s^{-1} and 10^{-4} m^2 s^{-1}, respectively (Blanke and Delecluse, 1993; Madec, 2008).

2.2 Biogeochemical model

The AS covers inshore nutrient-rich habitats where large-size classes phytoplankton such as diatoms dominate and more oligotrophic regions where small-size classes phytoplankton such as dinoflagelates dominate (Banse, 1994; Garrison et al., 1998). In order to account for this diversity, we used the intermediate complexity biogeochemical model Pelagic Interaction Scheme for Carbon and Ecosystem Studies (PISCES) that includes two phytoplankton size classes corresponding to diatoms and nanophytoplankton and two zooplankton size classes (Aumont et al., 2003; Aumont and Bopp, 2006). The original version of PISCES was simplified from 24 to 16 tracers, taking out compartments related to the cycling of phosphate and iron, which are not the major limiting nutrients in the Arabian Sea (Aumont et al., 2003; Moore

et al., 2004; Dutkiewicz et al., 2005; Koné et al., 2009). Oxygen and nitrate are initialised from the climatological fields derived from the model of Koné et al. (2009) (see Sect. 2.4) and other biological tracers were initially set to low values. As for temperature and salinity, nitrate and oxygen are relaxed to WOA05 values in the Bab el Mandeb, Hormuz and Malacca straits. To ensure positive values, biogeochemical tracers are advected with the positive Monotone Upstream-centered Schemes for Conservation Laws (Van Leer, 1979; Lévy et al., 2001) and dissipated along isopycnals at small scales by a Laplacian operator with a diffusion coefficient of 100 $m^2.s^{-1}$. Vertical mixing in the biogeochemical model is identical to the one in the physical model. Formulations and parameters are summarised in the Appendix of Resplandy et al. (2011).

2.3 Oxygen budget

The oxygen concentration in the model evolves according to

$$\partial_t \mathrm{O_2} = \underbrace{\left(\frac{\partial \mathrm{O_2}}{\partial t}\right)_{\mathrm{Dyn}}}_{\text{Dynamical transport}} + \underbrace{\left(\frac{\partial \mathrm{O_2}}{\partial t}\right)_{\mathrm{Bio}}}_{\text{Biological sources and sinks}} + J_{\mathrm{flux}}, \quad (1)$$

where $(\partial \mathrm{O_2}/\partial t)_{\mathrm{Bio}}$ denotes all biological processes affecting the concentration of O_2 (see Eq. 3), $(\partial \mathrm{O_2}/\partial t)_{\mathrm{Dyn}}$ summarises the processes that affect the dynamical transport of oxygen (see Eq. 4), and J_{flux} is the contribution of O_2 air–sea flux (see Eq. 7).

In the biogeochemical model PISCES, dissolved oxygen is a prognostic variable computed with the following equation:

$$\begin{aligned}\left(\frac{\partial \mathrm{O_2}}{\partial t}\right)_{\mathrm{Bio}} = & \underbrace{(R^1_{\mathrm{o:c}} + R^2_{\mathrm{o:c}})(\mu^P_{\mathrm{NO_3}} P + \mu^D_{\mathrm{NO_3}} D)}_{\text{New Production}} \quad (2)\\ & + \underbrace{R^1_{\mathrm{o:c}}(\mu^P_{\mathrm{NH_4}} P + \mu^D_{\mathrm{NH_4}} D)}_{\text{Regenerated Production}} - \underbrace{\lambda^*_{DOC} f(\mathrm{O_2})\mathrm{DOC}}_{\text{Remineralisation}}\\ & - \underbrace{G^Z Z - G^M M}_{\text{Respiration}} - \underbrace{R^2_{\mathrm{o:c}}\mathrm{Nitrif}}_{\text{Nitrification}}.\end{aligned}$$

Oxygen is produced during photosynthesis (calculating the uptake of nitrate and ammonium by phytoplankton separately) by nanophytoplankton (P) and diatoms (D) and consumed by dissolved organic matter (DOC) remineralisation, small (Z) and large (M) zooplankton respiration, and nitrification (Nitrif). The term Nitrif represents the conversion of ammonium into nitrate and is assumed to be photoinhibited and reduced in suboxic waters. It is therefore a function of the ammonium and oxygen concentrations and photosynthetically available radiation. In this formulation, stoichiometric ratios account for the change in oxygen relative to carbon during ammonium conversion into organic matter ($R^1_{\mathrm{o:c}}$) and during nitrification ($R^2_{\mathrm{o:c}}$). Their values have been set respectively to 140 : 122 and 32 : 122 so their sum equals the ratio for photosynthesis using nitrate proposed by Takahashi et al. (1985). A key process in modulating oxygen concentration in the model is the remineralisation of DOC. It can be either oxic or anoxic, depending on the local oxygen concentration. The splitting between the two types of organic matter degradation is performed using the factor $f(\mathrm{O_2})$ comprised between 0 and 1:

$$f(\mathrm{O_2}) = 1 - \min\left[1, 0.4\frac{\max[0,(6-\mathrm{O_2})]}{1+\mathrm{O_2}}\right]. \quad (3)$$

When $\mathrm{O_2} > 6\,\mu\mathrm{mol\,L^{-1}}$ ($f(\mathrm{O_2}) = 1$), remineralisation is stricly aerobic and only consumes oxygen. However, when $\mathrm{O_2} < 6\,\mu\mathrm{mol\,L^{-1}}$ ($f(\mathrm{O_2}) < 1$), part of the organic matter remineralisation consumes nitrate instead of oxygen (denitrification). Implicitly, degradation rates for respiration and denitrification are therefore identical.

DOC concentrations are highly dependent on the detrital particles distribution in the water column. To account for the range of particle sinking velocities observed in the ocean, the model distinguishes between small, slowly sinking particles (sinking rate of $\mathrm{m\,d^{-1}}$) and large particles with a depth-increasing sinking rate (50–200 $\mathrm{m\,d^{-1}}$). Aggregation and disaggregation processes, which are necessary for reproducing the observed increase in the relative abundance of large particles with depth and the presence of small particles at certain depths, is represented using a turbulence parameter and the concentrations of DOC and small and large detritus (see Appendix of Resplandy et al. (2011)).

The dynamical transport of oxygen is computed as

$$\left(\frac{\partial \mathrm{O_2}}{\partial t}\right)_{\mathrm{Dyn}} = - \underbrace{u_{\mathrm{H}} \cdot \nabla_H \mathrm{O_2}}_{\text{lateral advection}} - \underbrace{w \cdot \nabla_Z \mathrm{O_2}}_{\text{vertical advection}} + \underbrace{\frac{\partial K_z \partial \mathrm{O_2}}{\partial z^2}}_{\text{vertical mixing}}. \quad (4)$$

The relative importance of the mean and eddy-driven circulations on the oxygen concentration is estimated using the Reynold's decomposition, where the mean and eddy-driven components of the advective supply are separated:

$$\underbrace{\overline{(-u_H \cdot \nabla_H O_2)}}_{\text{lateral advection}} = \underbrace{\overline{(-u_H} \cdot \overline{\nabla_H \mathrm{O_2})}}_{\text{mean lateral advection}} + \underbrace{\overline{(-u'_H \cdot \nabla_H \mathrm{O'_2})}}_{\text{eddy lateral advection}} \quad (5)$$

and

$$\underbrace{\overline{(-w \cdot \nabla_Z \mathrm{O_2})}}_{\text{vertical advection}} = \underbrace{\overline{(-w} \cdot \overline{\nabla_Z \mathrm{O_2})}}_{\text{mean vertical advection}} + \underbrace{\overline{(-w' \cdot \nabla_Z \mathrm{O'_2})}}_{\text{eddy vertical advection}}, \quad (6)$$

where the over-bar denotes a time mean to be defined and the prime of all deviations from this time mean (referred as the eddy term). To exclude the contribution of seasonal variations from the eddy term and incorporate them into the mean term, we defined the mean state of $\overline{u_H}$, $\overline{w}$ and $\overline{\mathrm{O_2}}$ as the monthly, ten-year mean climatology of u_H, w and $\mathrm{O_2}$.

Finally, J_{flux} is the flux of O_2 from air to sea ($F_{\mathrm{O_2}}$) divided by the depth of model surface layer, where

$$F_{\mathrm{O_2}} = k_w(\alpha \mathrm{O_{2\,atm}} - \mathrm{O_2}), \quad (7)$$

k_w is the transfer velocity, $(\alpha O_{2\,atm} - O_2)$ is the difference in O_2 partial pressure between the air and surface sea water, and α the solubility of O_2 in seawater.

In this work, the terms $(\partial O_2/\partial t)_{Bio}$ and $(\partial O_2/\partial t)_{Dyn}$ are examined to estimate the biological and dynamical contributions to the seasonality and the formation of the OMZ in the Arabian Sea. J_{flux} is not discussed because it impacts the top-most level of the model and consequently only slightly modifies the concentration in the mixed layer located above the OMZ.

2.4 Model Equilibration

Equilibration of the oxygen and nitrate content in subsurface waters, where the OMZ is located, requires to carry experiments for several tens of years, which is out of reach with the resolution of the model. In order to circumvent this issue, the model spin-up is performed in two steps, first at 1 / 2° resolution (243 yr) and then at 1 / 12° (3 yr). More precisely, the global simulation of Koné et al. (2009), based on the same biogochemical model but with iron and phosphate compartments, provides the initial and the southern open boundary condition for nitrate and oxygen. The 1 / 12° resolution regional model was then integrated from 1992 to 2003 and we focus our analysis on a model climatology built by averaging from 1995 to 2003. The first 3 yr were taken out to remove the transition due to the change in resolution. This method does not allow complete equilibration but reduces the model drift to a level that is below the magnitude of the processes analysed in this study. Hence, the biological ($(\partial O_2/\partial t)_{Bio}$ in Eq. 1) and dynamical ($(\partial O_2/\partial t)_{Dyn}$ in Eq. 1) contributions to the oxygen budget in our model run are not in perfect balance. The model is linearly drifting with a trend of the order of 0.01 µmol L^{-1} $month^{-1}$ on average between 200 and 1500 m (not shown).

The biological and dynamical annual trends are both maximum on the western side of the AS, where they tend to balance each other (Fig. 2a and b). The residual term $(\partial O_2/\partial t)$ is < 0.02 µmol L^{-1} $month^{-1}$ on average between 200 and 1500 m (Fig. 2c), which represents an annual difference < 0.5 % of the O_2 concentration. Note that the regional average of this residual term corresponds to the model drift of ~ 0.01 µmol L^{-1} $month^{-1}$ discussed above. The spatial patterns in this residual term primarily arises from the presence of internal variability (the signature of eddies is still apparent in the long-term mean of the dynamical trend) and interannual variability.

3 Model evaluation

Here, we focus on the model's ability to reproduce the OMZ and its seasonal variations. Dynamical and biological features essential to understand the oxygen budget are also briefly described. A detailed evaluation of the model's ability to simulate the seasonal cycle of circulation, mixed layer depth, nutrients concentrations and phytoplankton can be found in Resplandy et al. (2011).

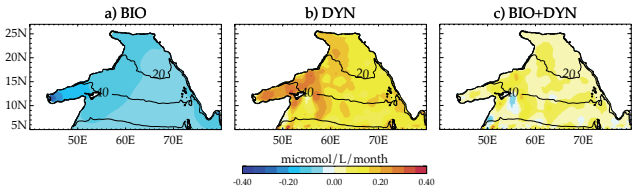

Fig. 2. Simulated annual trends of oxygen averaged between 200 and 1500 m: **(a)** biological trend $\left(\frac{\partial O_2}{\partial t}\right)_{Bio}$, **(b)** dynamical trend $\left(\frac{\partial O_2}{\partial t}\right)_{Dyn}$ and **(c)** residual $\left(\frac{\partial O_2}{\partial t}\right) = \left(\frac{\partial O_2}{\partial t}\right)_{Bio} + \left(\frac{\partial O_2}{\partial t}\right)_{Dyn}$. Units are in µmol L^{-1} $month^{-1}$. Contours indicate the oxygen concentration in µmol L^{-1} averaged between 200 and 1500 m.

3.1 Main dynamical and biological features

In the Arabian Sea, the monsoon system leads to the semi-annual reversal of the oceanic circulation. The two resulting monsoons drive two seasonal phytoplanktonic blooms (Banse, 1987; Wiggert et al., 2005; Lévy et al., 2007). During the Northeast Monsoon (NEM, December–February), relatively strong, cool and dry winds blow southwest across the Arabian Sea, forcing a counterclockwise circulation and inducing a significant ocean heat loss (Fig. 1a). The resulting convective mixing (Bauer et al., 1991; Weller et al., 2002) entrains nutrient-rich waters, triggering a phytoplankton bloom north of 15° N (Madhupratap et al., 1996) (Fig. 1c and e). During the late stages of the Spring Intermonsoon (SIM, March–May) and the Southwest Monsoon (SWM, June-August), the wind and oceanic circulations reverse (Fig. 1b). The main oceanic features associated with the strong southwesterly wind jet of warm and moist air or Findlater Jet (Findlater, 1969) are the coastal upwelling systems that develop along the western (Brock and McClain, 1992; Veldhuis et al., 1997; Hitchcock et al., 2000) and eastern (Banse, 1968; Lierheimer and Banse, 2002) coasts of the Arabian Sea. Strong positive vertical velocities upwell nutrients into the euphotic layer, enhancing phytoplankton production (Fig. 1d and f). These major features of the monsoon periods are modulated by a strong lateral contrast in Ekman pumping (Fig. 1a and b). While NEM winds favour downwelling in the northwest and upwelling in the southwest, the SWM Findlater Jet triggers open-ocean upwelling north of the Findlater Jet and a downwelling to the south (Bauer et al., 1991; Rao et al., 1989; Schott and McCreary, 2001; Fischer et al., 2002; Weller et al., 2002). During the Spring and Fall Intermonsoons (SIM, March–May; FIM, September–November respectively), winds and ocean currents are reversing and become much weaker.

The main achievement of our relatively high horizontal resolution (1 / 12°) model was to successfully simulate the mesoscale spatial variability (Fig. 3). This improved the representation of the two seasonal blooms (Fig. 1e and f) by (1) enhancing vertical advection of nutrients in the early stage of upwelling and strengthening the offshore transport of nutrients into the central Arabian Sea during the summer monsoon, and (2) by mesoscale vertical advection of nutrients in the central Arabian Sea during the winter monsoon.

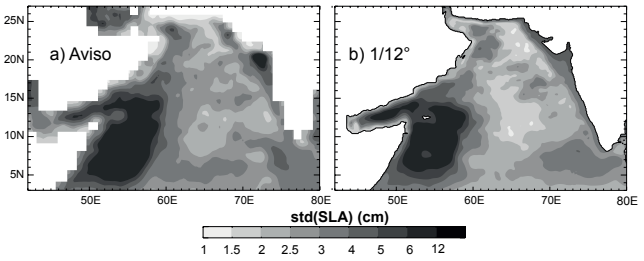

Fig. 3. (a) Mesoscale circulation estimated from the AVISO dataset and **(b)** in the model at eddy-resolving resolution. The mesoscale circulation is quantified by the standard deviation of the sea level anomaly (SLA) filtered in the 14–120 days band, over the 1995–2003 period.

3.2 Oxygen concentration in OMZ

Here, we examine how the OMZ and its seasonality in the model compare to the World Ocean Atlas 2009 (WOA09). We distinguish three depth ranges of the OMZ: the "core" delimited by the 20 µmol L^{-1} isoline (Paulmier and Ruiz-Pino, 2009); the "upper OMZ" between the 100 µmol L^{-1} and 20 µmol L^{-1} isolines that extends from the oxycline to the core; and the "lower OMZ" between the 20 µmol L^{-1} and 100 µmol L^{-1} isolines located at the base of the OMZ.

The core of the OMZ is confined to the enclosed part of the basin north of 10°N and roughly spreads vertically between 200 and 1000 m (Figs. 1g, h and 4a, c). The core presents an east–west contrast with lower oxygen concentrations at the centre of the basin and higher concentrations along the west and east coasts of the Arabian Sea (Figs. 1g, h and 4a). The vertical extension of the core is particularly reduced along the west coast of the Arabian Sea where waters with oxygen concentrations lower than 20 µmol L^{-1} are only observed below 400 m (Fig. 4a). The OMZ is thus shifted eastward from the region of highest biological production located along the west coast of the Arabian Sea (Fig. 1c–f).

The main characteristics of the OMZ are reproduced by the model. Oxygen concentrations are however slightly larger than observed in the upper OMZ ($\sim$ 100 m depth) and along the west coast of the Arabian Sea, inducing a reduction of the core's volume and an overestimation of the eastward shift of the OMZ (Figs. 1g–j and 4). More quantitatively, the volume of core waters in the Arabian Sea is of the order 1.5×10^{15} m^3 in the model, whereas it is of 1.8×10^{15} m^3 in the WOA09. In contrast, the volume of waters with concentrations lower than 60 µmol L^{-1} give a similar estimate of 4×10^{15} m^3 in the model and the WOA09. In fact, what the model does not represent adequately is the strong oxygen gradient in the oxycline (Fig. 4). This bias most probably arises from the relatively low vertical resolution in the model (46 vertical levels with 10 levels between 50 and 300 m) that is insufficient to properly resolve the sharp oxygen gradient of the oxycline (Fig. 4). Along the west coast of the Arabian Sea, oxygen concentrations between 400 and 1000 m are ≥ 30 µmol L^{-1} in the model, whereas concentrations ≤ 20 µmol L^{-1} are observed (see contours in Fig. 4a and b). This overestimation of the eastward shift in the model however confirms that this feature is simulated and maintained in the model and is not only arising from initial conditions.

Despite the relatively low number of observations in the World Ocean Atlas (particularly below 200 m) (Bianchi et al., 2012), seasonal variations of oxygen concentrations can be detected in the WOA09 climatology (Fig. 5a and c). The oxycline is uplifted by $\sim$50-100 m along the western, eastern and northern coasts, where upwelling occurs during the SWM (see 100 µmol L^{-1} isoline in Fig. 5a and c). The depth of the oxycline is also modulated seasonally in the central Arabian Sea. As indicated by the 100 µmol L^{-1} isoline, the oxycline domes in the southeast (south of 15° N and east of 65° E, Fig. 5 a and c) and is deepened in the northwest (north of 20°N and west of 60° E, Fig. 5a and c) during the NEM, while the opposite is observed during the SWM. At depth, the seasonality is very weak, with the 100 µmol L^{-1} isoline located around 2000 m being slightly uplifted during the SWM in comparison to its depth during the NEM (Fig. 5a and c). Note, however, that some of the observed seasonal changes are to be considered with extreme caution given the few observations available in WOA09. The model captures the major seasonal features, including the variations of the oxycline depth and the intensification of the eastward shift during the SWM (Fig. 5b and d). However, the two model biases described previously also affect the representation of the seasonal variability: the weaker oxygen vertical gradient in the oxycline results in weaker variations of the oxycline depth (Fig. 5b and d); and the increase in oxygen concentration along the west coast of the Arabian Sea during the SWM extends further vertically and laterally offshore (Fig. 5b).

4 Results

The annual budget of dynamical and biological trends of oxygen presented in Fig. 2 averages the contributions of sources and sinks that are highly variable and sometimes with opposed effects over the OMZ depth range and over a seasonal cycle. For example, the oceanic circulation that

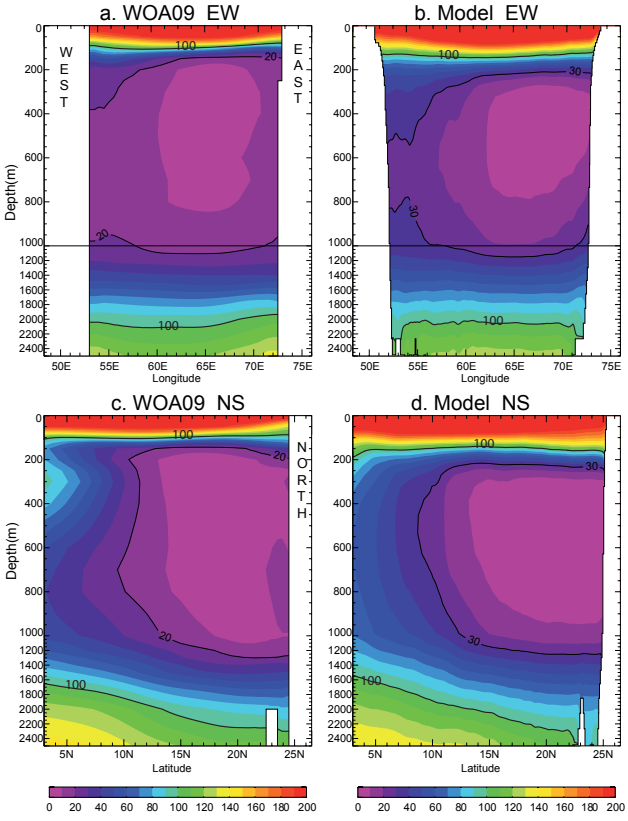

Fig. 4. Annual oxygen concentration (in µmol L^{-1}) along the east–west (EW) and north–south (NS) sections indicated in Fig. 1h in **(a)** WOA09 climatology and **(b)** the model.

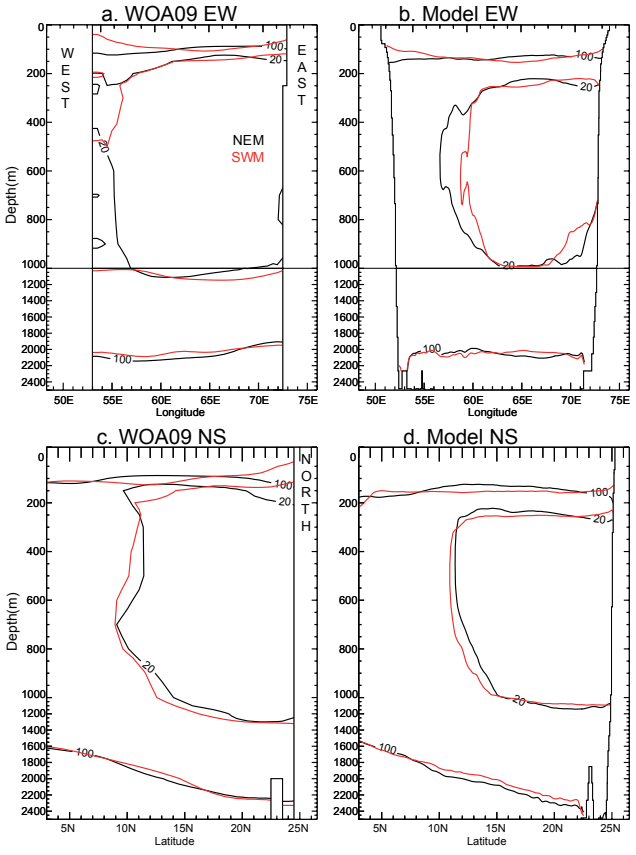

Fig. 5. Seasonal variability of the OMZ's core (20 µmol L^{-1} contour) and of the 100 µmol L^{-1} isoline along the east–west (EW) and north–south (NS) sections indicated in Fig. 1h. Contours are given for the winter (NEM in black) and summer (SWM in red) monsoons in **(a)**, **(c)** WOA09 climatology and **(b)**, **(d)**. the model

reverses semiannually tends to cancel out on annual average but can still influence the oxygen budget due to the non-linearities associated with the transport of oxygen (or any other tracer). To disentangle the effect of the different sources and sinks of oxygen in the annual balance, we first examine their contribution over one climatological seasonal cycle and over the OMZ depth range in three regions of contrasted dynamical and biological context (Sect. 4.1). Then, we examine the annual impact on the OMZ of the prominent dynamical processes identified in the three sub-regions and quantify the proportion of these processes associated with the presence of mesoscale eddies (Sect. 4.2).

4.1 Drivers of oxygen seasonality

Here, the seasonality of the dynamical and biological processes modulating the oxygen concentration (Sect. 2.3) and their impact on the OMZ are examined. The oxygen concentration in the Arabian Sea displays a seasonal cycle that roughly peaks during the SWM and NEM periods (Fig. 5 and Sect. 3). In the upper OMZ, the seasonality can reach 15 % of the total oxygen concentration (amplitude of annual variations of ~ 6 µmol L^{-1} for an annual mean oxygen concentration of 40 µmol L^{-1}), whereas in the core and the lower part of the OMZ it is ≤ 5 % (amplitude of annual variations of ~ 1–3 µmol L^{-1} compared to an annual-mean oxygen concentration of 20–40 µmol L^{-1}). In the following we examine this seasonality by quantifying the seasonality of the biological and dynamical trends in the O_2 equation (Eqs. 1, 3 and 4). The contributions of vertical and horizontal advection to the dynamical transport of oxygen are detailed, whereas vertical mixing that is much smaller below 200 m is not presented. We focus on three regions of the OMZ (defined in Fig. 1j) with contrasted biological and dynamical processes: the first region is located offshore in the central Arabian Sea (noted CAS), where the OMZ's core is most intense; the second is along the coast of Oman (noted OMA), where the coastal upwelling and the biological activity are the strongest; and finally, the region along the southwest coast of India (noted IND), which presents a relatively weak coastal upwelling but is under the strong influence of coastal Kelvin and Rossby waves (Han et al., 2011).

As expected, biological consumption in these three regions is confined to the upper 300 m (Figs. 6, 7 and 8 panels a).

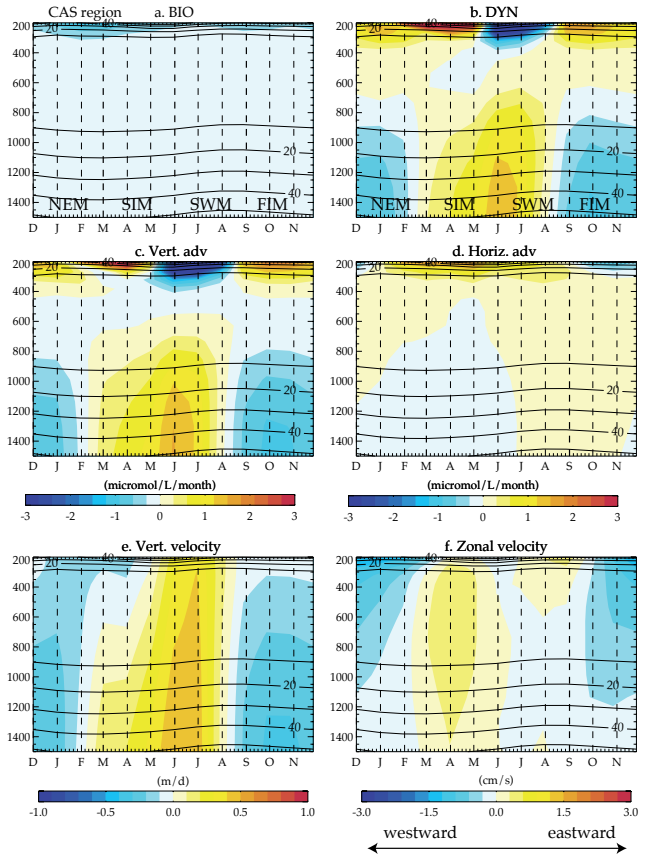

Fig. 6. Seasonality in CAS region (see Fig. 1j) between 200 and 1500 m in the model. **(a–d)** Components of the oxygen budget (μmol L^{-1} month^{-1}) with the biological trend $\left(\frac{\partial O_2}{\partial t}\right)_{\text{Bio}}$ **(a)**, the dynamical transport $\left(\frac{\partial O_2}{\partial t}\right)_{\text{Dyn}}$ **(b)**, and the contributions of vertical advection **(c)** and horizontal advection **(d)** to the dynamical transport **(e)** vertical velocity (m d^{-1}). **(f)** Zonal component of horizontal velocity (cm s^{-1}), where values > 0 (< 0) indicate eastward (westward) velocities. Contours indicate the oxygen concentration in the region (μmol L^{-1}).

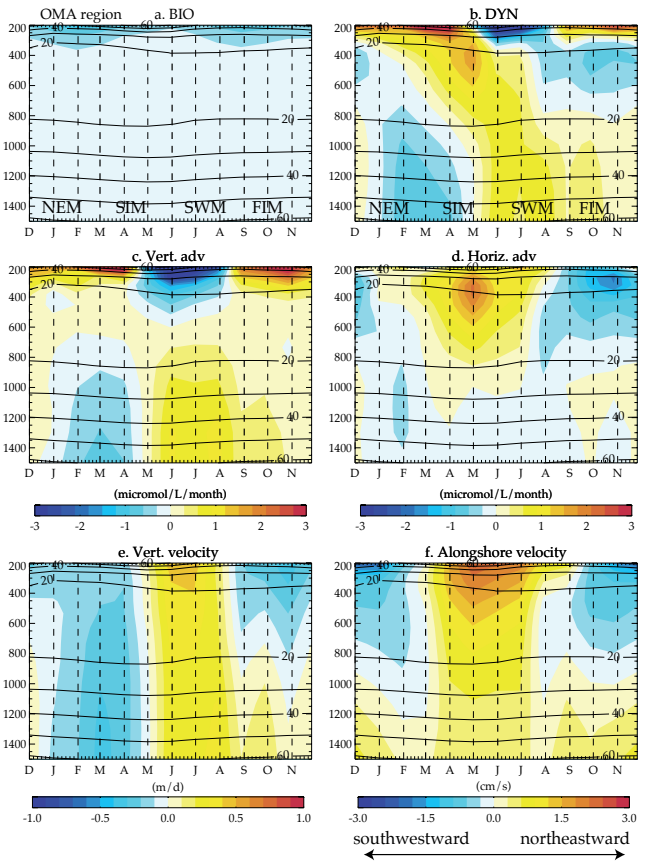

Fig. 7. Seasonality in OMA region (see Fig. 1j) between 200 and 1500 m in the model. **(a–d)** Components of the oxygen budget (μmol L^{-1} month^{-1}) with the biological trend $\left(\frac{\partial O_2}{\partial t}\right)_{\text{Bio}}$ **(a)**, the dynamical transport $\left(\frac{\partial O_2}{\partial t}\right)_{\text{Dyn}}$ **(b)**, and the contributions of vertical advection **(c)** and horizontal advection **(d)** to the dynamical transport **(e)** vertical velocity (m d^{-1}). **(f)** Alongshore component of horizontal velocity (cm s^{-1}), where values > 0 (< 0) indicate northeastward (southwestward) velocities. Contours indicate the oxygen concentration in the region (μmol L^{-1}).

In the three regions, the biological trend is maximal during the monsoonal productive periods that peak in January–February and August–September. The dynamical trend counteracts the biological uptake by ventilating the upper OMZ from September to May in CAS and OMA and from June to November in IND (Figs. 6, 7 and 8 panels b), which support some of the conclusions of Sarma (2002). However, the amplitude of the dynamical trend in our model is by far larger than the biological contribution, which does not support the hypothesis of Sarma (2002) of a compensation between the dynamical input of oxygen and the biological uptake of oxygen during each season. The biological and dynamical trends do compensate on annual average (see Sect. 2.4 and Fig. 2) but their imbalance on seasonal scales explains the seasonality of oxygen concentrations in the model. These seasonal variations of the dynamical transport of oxygen reflect the major circulation features associated with the monsoonal system, which are different depending on the regional context.

In the central Arabian Sea (CAS) region, the seasonal changes in the upper and lower OMZ are roughly anti-correlated, with oxygen concentration increasing (decreasing) in the upper OMZ and decreasing (increasing) in the lower OMZ in FIM-NEM (in late SIM-SWM) (Fig. 6b). This seasonality primarily arises from the vertical advection of oxygen associated with Ekman pumping (Fig. 1a and b). During the FIM and NEM periods, negative vertical velocities transport surface ventilated waters below 200 m and slightly deepen the core of the OMZ (Fig. 6c and e). During the late SIM and SWM periods, positive Ekman pumping

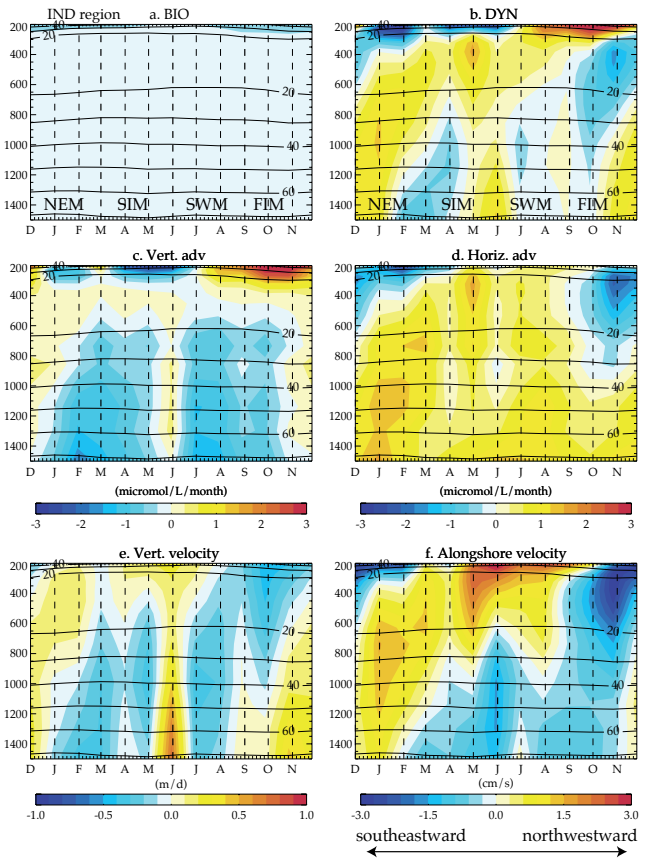

Fig. 8. Seasonality in IND region (see Fig. 1j) between 200 and 1500 m in the model. **(a–d)** Components of the oxygen budget (μmol L^{-1} $month^{-1}$) with the biological trend $\left(\frac{\partial O_2}{\partial t}\right)_{Bio}$ **(a)**, the dynamical transport $\left(\frac{\partial O_2}{\partial t}\right)_{Dyn}$ **(b)**, and the contributions of vertical advection (**(c)** and horizontal advection **(d)** to the dynamical transport **(e)** vertical velocity (m d^{-1}). **(f)** Alongshore component of horizontal velocity (cm s^{-1}), where values > 0 (< 0) indicate northwestward (southeast ward) velocities. Contours indicate the oxygen concentration in the region (μmol L^{-1}).

upwells the water column, resulting in reduced oxygen concentration between 200 and 400 m and enhanced concentrations below (Fig. 6c and e). The contribution of horizontal advection in CAS is most intense in the upper OMZ between 200–300 m (Fig. 6d, f and h). During the NEM, slightly higher oxygen concentrations located along the Indian coast are advected westward into the CAS (Fig. 6f), whereas during the SIM and SWM more ventilated waters from the upper OMZ along the west coast of the Arabian Sea are advected eastward (Fig. 6f).

The oxygen budget in the upwelling region of Oman (OMA) is also influenced by the dynamical signature of Ekman pumping (Fig. 7c). The impact of the summer intense pumping (occurring between May and July) is counterbalanced by downwelling during the rest of the year (Fig. 7e). It is interesting to highlight that the vertical advection associated with the coastal upwelling active during the late-SIM and SWM periods is confined to the surface and therefore does not visibly impact the oxygen concentration below 200 m. The impact of vertical advection in OMA is significantly modulated by the contribution of horizontal advection that extends down to 800 m throughout the year (Fig. 7d). During SIM and SWM periods, oxygenated waters are advected northeastward into OMA (Fig. 7f). This feature that impacts OMA and more generally the western coast of the Arabian Sea is associated with the intense western boundary current or Somali Current that flows northward at that period of the year (SC in Fig. 1b). During the FIM and NEM periods, the circulation reverses (Fig. 1h). Low-oxygen waters originated from the north, where the OMZ is more intense, are horizontally advected into OMA (Fig. 7f). Note that the supply of oxygenated southern waters during the SIM and SWM periods is larger than the advection of low-oxygen waters from the northern Arabian Sea during the FIM and NEM periods (Fig. 7d), which is in agreement with the high annual biological uptake of oxygen in the upwelling region of Oman (Figs. 2 and 7a).

The oxygen transport in the upwelling region southwest of India (IND) is largely influenced by horizontal advection (Fig. 8b and d). The horizontal advection between 200 and 1500 m is dominated by the coastal undercurrent that spreads below 150 m (Fig. 8f) and flows alongshore in the opposite direction from the surface current (Figs. 8f and 9a). During the SIM and SWM periods, the northwestward undercurrent transports oxygen-rich waters located south of the tip of India into the Arabian Sea. During the FIM and NEM, the circulation reverses and the undercurrent transports low-oxygen waters originated from the northern Arabian Sea southeastward into the IND region (Fig. 8d and f). The oxygen budget is also under the influence of vertical advection with a strong contribution of Ekman pumping in May–June (Fig. 8c and e). A striking feature of the seasonality in the IND region is the intense modulation of the local processes described above by remote forcing (Fig. 8b). Unlike in CAS and OMA where the variability of the velocity fields is in phase in the upper and lower OMZ, the vertical and horizontal velocity fields in IND display a vertical propagation with a semiannual ($\sim$ 180-day) phase (Fig. 8e and f), strongly suggesting the influence of second baroclinic mode waves. In addition, the seasonality of the alongshore wind stress is very weak in the IND region and cannot explain the upwelling onset (identified with the sea level anomaly) or the seasonal changes in direction of the surface current and undercurrent (Fig. 9a). These processes are generally attributed to coastal Kelvin waves known to propagate from the Bay of Bengal into the Arabian Sea (McCreary et al., 1993; Nethery and Shankar, 2007; Han et al., 2011). Finally, the sea level anomaly in the model highlights the westward propagation of Rossby waves generated along the southeastern coast of India into the Arabian Sea (Fig. 9b).

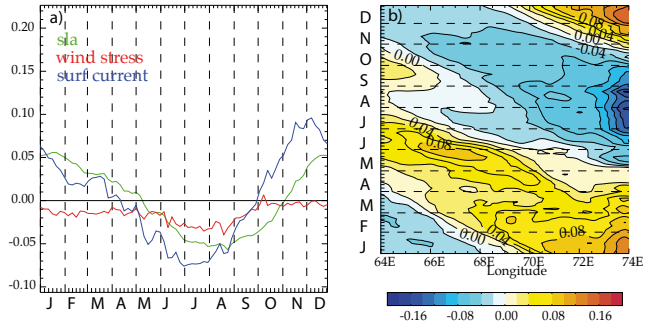

Fig. 9. Remote forcing in IND region. **(a)** Seasonality of alongshore surface current ($m\,s^{-1}$, positive (negative) values indicate northwestward (southeastward) flow), sea level anomaly (m) and wind stress ($m^{-2}\,s^{-2}$). **(b)** The time–longitude section of sea level anomaly (m) between January and December, highligting the westward propagation of Rossby waves generated along the southwestern coast of India.

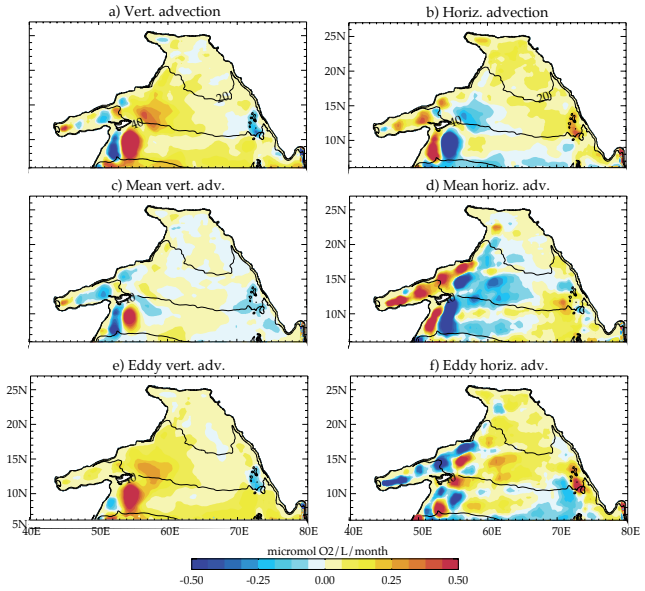

Fig. 10. Simulated annual trends of oxygen between the 200 and 1500 m: **(a)** vertical advection, **(b)** horizontal advection, **(c)** mean vertical advection, **(d)** mean horizontal advection, **(e)** eddy-driven vertical advection and **(f)** eddy-driven horizontal advection. Units are in $\mu mol\,L^{-1}\,month^{-1}$. Contours delimits the 20, 40 and 60 $\mu mol\,L^{-1}$ oxygen concentration on average between 200 and 1500 m.

4.2 Annual advective sources and sinks of oxygen in OMZ

The previous section detailed the processes dominating the oxygen budget in three key regions of the OMZ during a seasonal cycle and over the vertical. We find that advective processes dominate the seasonality in the three subregions. However, the dynamical trend of oxygen roughly balances the biological uptake (Fig. 2). Here, we examine how these processes counterbalance each other over annual time scales and over the OMZ depth range. The contribution of mesoscale eddies to the advection of oxygen is also investigated using the reynolds averaging method to separate the transport of oxygen associated with the eddy-driven and the mean circulations (see Sect. 2.3).

The averaged vertical and horizontal advection of oxygen show contrasted spatial distributions (Fig. 10a and b). The supply of oxygen to the OMZ is mostly sustained by vertical advection in the southwest and by horizontal advection in the northeast and along the western coast of the Arabian Sea. This is in agreement with the processes identified in the three selected regions: the combination of large vertical and horizontal advection of oxygen in OMA; the major role of horizontal advection in IND; and the contribution of horizontal advection in CAS. However, one major difference that arises from the annual and vertical integration of advective terms is the role of Ekman pumping. Whereas Ekman pumping (which is the major component of the mean vertical advection in the OMZ) was a key process in the oxygen budget seasonality, its contribution averaged annually over the OMZ depth range is much smaller (Fig. 10c). Indeed, the vertical transport associated with Ekman pumping compensates both temporally and vertically: the semiannual reversal of monsoonal winds leads to opposed oxygen trends during the SWM and NEM, and the vertical displacement of the OMZ results in opposed trends in the upper and lower OMZ (Fig. 6c). Consequently, the oxygen concentration in the OMZ is mostly supplied vertically by mesoscale eddies (Fig. 10e). The vertical component of eddy-driven advection supplies oxygen to the OMZ depth range in most regions of the Arabian Sea but is most intense in the vicinity of the Somali Current, where the energetic dynamics of the western boundary current is a major generator of mesoscale structures (Figs. 10e and 3b). This vertical supply of oxygen occurs both across the oxycline and in the lower part of the OMZ (not shown). Indeed, the Great Whirl and the other mesoscale structures associated with the Somali Current combine a deep vertical extension (Schott and McCreary, 2001) and high vertical velocities (Resplandy et al., 2011).

The mean horizontal circulation supplies most of the oxygen in a coastal band along the western coast of the Arabian Sea (Fig. 10d). Indeed, despite the monsoonal reversal (Fig. 1a and b), the effect of the SWM boundary current that transports oxygenated waters from southern origin along the western coast of the Arabian Sea dominates the annual mean circulation. Further offshore the mean horizontal advection supplies oxygen-poor waters (Fig. 10d). The dominant effect here is the transport of low-oxygen concentrations from the OMZ by an anti-cyclonic gyre circulation compensating the northward advection along the western boundary current. In the central Arabian Sea, weak annual averaged currents flow westward and advect waters originating from

the core of the OMZ to the western Arabian Sea. This westward transport of low-oxygen waters is, however, partly compensated by eddy-driven horizontal advection that supplies oxygen to the OMZ (Fig. 10b and f). The eddy-driven horizontal advection of oxygen supplies oxygen mostly in the central Arabian Sea and more particularly offshore Oman and India (Fig. 10f). In these regions, baroclinic instabilities enhanced by the bathymetry and the presence of upwelling systems during the SWM promote the formation of mesoscale structures (Fig. 3). The eddy-driven horizontal transport of oxygen offshore Oman is sustained by 100 km width mesoscale filaments extending 500–1000 km into the Arabian Sea, whereas offshore India it is mostly mediated by mesoscale eddies of 50–100 km and the 10–50 km width filaments wrapped around them (see Resplandy et al. (2011) for further details on modelled and observed mesoscale structures).

5 Discussion and conclusions

In this study, we examined the factors controlling the sources and sinks of oxygen in the OMZ of the Arabian Sea using an eddy-resolving biophysical model. The main results focus on the modulation of these processes by the monsoon seasonality and by mesoscale eddies. As expected, the biological consumption of oxygen is most active in the northern and western Arabian Sea and in a narrow band along the coast of India, which are the regions where the winter and summer monsoonal blooms occur. In our model the biological consumption of oxygen in the western Arabian Sea is counterbalanced by the supply of oxygen by horizontal and vertical advection. The western boundary current or Somali Current horizontally transports oxygenated waters coming from the south along the western coast of the Arabian Sea. This contribution of the mean currents to the oxygen transport is essential in the coastal area off Oman and Somalia. In the other regions of the Arabian Sea, the eddy-induced advection tends to destroy the OMZ. The predominant effect of mesoscale structures is the vertical supply of oxygen to the OMZ across the oxycline and at its base and the lateral export of ventilated waters offshore the upwelling of Oman. The eddy-induced vertical advection supplies oxygen originating from the surface and the deep ocean over most of the OMZ area. This ubiquitous impact of eddies on the vertical advection of oxygen is associated with the numerous eddies that populate the northern Arabian Sea during the winter monsoon (Fischer et al., 2002; Resplandy et al., 2011). The contribution of eddy vertical advection is, however, stronger offshore the western boundary upwelling of Oman and Somalia, where highly energetic mesoscale structures (mainly the Great Whirl and the Socotra Eddy) develop during the summer monsoon. This significant impact of eddies on the vertical advection of oxygen is explained by the intense vertical velocities associated with the ageostrophic dynamics of eddies (Klein et al., 2008; Lévy et al., 2010).

The role of mesoscale eddies on the horizontal advection of oxygen is most intense offshore the upwelling of Oman. Oxygenated waters brought along the western coast of the Arabian Sea by the Somali Current are redistributed into the central Arabian Sea by $\sim$ 100 km width mesoscale filaments extending $\sim$ 500–1000 km offshore. These filamentary structures extend down to $\sim$ 200–300 m and their impact on the oxygen transport is therefore mostly confined to the upper OMZ. Eddy horizontal advection is also the major source of oxygen along the southwestern Indian coast. This region is populated with mesoscale eddies of 50–100 km, which are constant features of eastern boundary upwelling (Marchesiello et al., 2004; Chaigneaun et al., 2009).

The major role of northward lateral advection and eddy-induced vertical advection in controlling the supply of oxygen to the OMZ is in agreement with the study of McCreary et al. (2012). In a suite of sensitivity experiments, they identified the horizontal transport of oxygenated waters from the south and the additional vertical mixing induced by eddies as essential to properly resolve the OMZ. In contrast, they found that horizontal mixing associated with eddies is not needed, which is in apparent contradiction with our finding that eddy-driven horizontal advection is a key process in supplying oxygen to the western central Arabian Sea and the southwestern Indian coast. This difference probably arises from the spatial resolution and the subsequent representation of eddies in the two models. Whereas mesoscale eddies are explicitly resolved in our model, they are parameterised by an enhanced mixing process and not an advective process in the model of McCreary et al. (2012). Although their parameterisation of enhanced mixing takes into account the spatial patterns of the eddy kinetic energy observed by satellite, it is unable to represent the horizontal transport mediated by the 1000 km long mesoscale filaments emanating from the coast of Oman or by the eastward propagating mesoscale eddies formed along the coast of India. The role of these structures in exporting upwelled waters and nutrients offshore was quite well described (Brock et al., 1991; Keen et al., 1997; Brink et al., 1998; Manghnani et al., 1998; Lee et al., 2000; Kawamiya, 2001; Resplandy et al., 2011) but their contribution to the oxygen budget in the Arabian Sea has not yet been assessed.

The seasonality detected in observations is weak and the sampling scarcity makes it difficult to assess if changes are really associated with the seasonality rather than with the low spatio–temporal sampling. However, the good agreement between the changes in oxygen concentration in observations and in the model gives us confidence that the OMZ responds to the monsoonal seasonality (Fig. 5). In agreement with previous findings, we find that the seasonality of the oxygen concentration in the OMZ is weak and of the order of 5 % of the annual mean oxygen concentration, except in the oxycline where it reaches 15 %. The seasonality in the model

results from an imbalance between oxygen advection and biological consumption. On an annual basis the biological uptake is indeed compensated by the dynamical transport of oxygen, but this is not the case if seasons are considered separately. The biological uptake of oxygen is most intense in the upper 300 m during the winter and summer monsoons, but its contribution to the simulated oxygen budget within the OMZ is 3 to 5 times lower than that due to the advection. On average, over the basin as well as on the regional scale, the strong seasonality in the factors controlling the oxygen concentration and the balance between the biological and dynamical processes on annual timescale do not support the hypothesis of a compensation between physical ventilation and remineralisation that has been put forward to explain the low variability of the OMZ on seasonal timescale (Sarma, 2002).

Most of the seasonality in the oxygen concentration in the central Arabian Sea, where the oxygen deficiency is most pronounced, arises from the effect of Ekman pumping and therefore results in a vertical displacement of the OMZ upper and lower boundaries. This result is in agreement with oxygen profiles from an ARGO float that captured vertical displacement of the oxycline of the order of 60–80 m (Prakash et al., 2012). In the northwestern Arabian Sea, the OMZ is downlifted during fall and winter and then uplifted during late spring and summer. This result is also supported by World Ocean Atlas observations that highlight a deepening (shallowing) of the oxycline in the central Arabian Sea during winter (summer) (Fig. 5). In coastal areas of the OMZ where upwelling occurs, horizontal advection also contributes to the oxygen seasonality. Along the Omani coast, the lateral transport of southern oxygen-rich waters by the western boundary current during summer is partly counterbalanced by the southward advection of oxygen-poor waters originated from the OMZ during fall and winter. This contribution of horizontal advection extends from the oxycline to 800 m depth, with the largest impact on the oxygen concentration between 200 and 500 m. Along the southwestern Indian coast, the OMZ is under the influence of the coastal undercurrent flowing below 150 m depth in the opposite direction of the surface monsoonal circulation (Shetye et al., 1990). Oxygen-rich waters coming from the south are thus advected toward the OMZ during summer and oxygen-poor waters originated from the OMZ are advected southward during winter. This result is in very good agreement with oxygen observations sampled during three cruises in winter, spring and summer that highlighted a large drawdown of oxygen during winter (de Sousa et al., 1996). In addition, our model evidenced a significant role of remote forcing on the oxygen budget along the southwestern coast of India. Lateral and vertical advection of oxygen are modulated seasonally by coastal Kelvin waves and westward-propagating Rossby waves. The fact that most of the seasonality in the oxygen concentration arises from the vertical displacement of the OMZ by Ekman pumping explains why the variability of the vertically-integrated content of oxygen is low. In addition, the semiannual reversal of monsoonal winds results in opposed oxygen trends during the summer and winter monsoons that partly compensate on annual average. However, the presence of low-oxygen waters at shallow depth during some parts of the year could impact the biogeochemistry in the region. As pointed out by Prakash et al. (2012), oxygen changes in surface waters could have direct environmental consequences, including the loss of habitat for high-oxygen-demand species and the modulation of greenhouse gases (N_2O and CO_2) outgasing.

Acknowledgements. We sincerely thank Jay McCreary and Jerome Vialard for their usefull comments on that paper. We thank the NEMO system team for their development and maintenance of the NEMO ocean general circulation model. Support was provided by the TANGGO (Toward AN Eddying Global Green Ocean) and EU FP7 project CARBOCHANGE Changes in carbon uptake and emissions by oceans in a changing climate, which received funding from the European Commissions Seventh Framework Programme under grant agreement no. 264879. Chl data were provided by the SeaWiFS Project and NASAs DAAC. Altimeter products were produced by Ssalto/Duacs and distributed by AVISO with support from Cnes (Centre National d'Etudes Spatiales).

Edited by: B. Dewitte

The publication of this article is financed by CNRS-INSU.

References

Aumont, O. and Bopp, L.: Globalizing results from ocean in situ iron fertilization studies, Global Biogeochem. Cy., 20, GB2017, doi:10.1029/2005GB002591, 2006.

Aumont, O., Maier-Reimer, E., Blain, S., and Monfray, P.: An ecosystem model of the global ocean including Fe, Si, P colimitations, Global Biogeochem. Cy., 17, 1060, doi:10.1029/2001GB001745, 2003.

Banse, K.: Hydrography of the Arabian Sea Shelf of India and Pakistan and effects on demersal fishes, Deep-Sea Research and Oceanographic Abstracts, 15, 45–48, IN7–IN10, 49–79, doi:10.1016/0011-7471(68)90028-4, 1968.

Banse, K.: Seasonality of phytoplankton chlorophyll in the central and northern Arabian Sea, Deep-Sea Res. Pt. I, 34, 713–723, doi:10.1016/0198-0149(87)90032-X, 1987.

Banse, K.: On the coupling of hydrography, phytoplankton, zooplankton, and settling organic particles offshore in the Arabian Sea, P. Indian AS-Earth, 103, 125–161, 1994.

Barnier, B., Madec, G., Penduff, T., Molines, J., Treguier, A., Sommer, J. L., Beckmann, A., Biastoch, A., Boning, C., Dengg, J.,

Derval, C., Durand, E., Gulev, S., Remy, E., Talandier, C., Theetten, S., Maltrud, M., McClean, J., and Cuevas, B. D.: Impact of partial steps and momentum advection schemes in a global ocean circulation model at eddy permitting resolution, Ocean Dynam., 56, 543–567, doi:10.1007/s10236-006-0082-1, 2006.

Bauer, S., Hitchcock, G. L., and Olson, D. B.: Influence of monsoonally-forced Ekman dynamics upon the surface-layer depth and plankton biomass distribution in the Arabian Sea, Deep-Sea Res., 38, 531–553, 1991.

Bianchi, D., Dunne, J. P., Sarmiento, J. L., and Galbraith, E. D.: Data-based estimates of suboxia, denitrification, and N_2O production in the ocean and their sensitivities to dissolved O_2, Global Biogeochem. Cy., 26, GB2009, doi:10.1029/2011GB004209, 2012.

Blanke, B. and Delecluse, P.: Variability of the tropical atlantic ocean simulated by a general circulation model with two different mixed-layer physics, J. Phys. Oceanogr., 23, 1363–1388, 1993.

Brink, K., Arnone, R., Coble, P., Flagg, C., Jones, B., Kindle, J., Lee, C., and Phinney, D.: Monsoons boost biological productivity in Arabian Sea, Eos Trans. AGU, 79, 165–169, doi:10.1029/98EO00120, 1998.

Brock, J. C. and McClain, C. R.: Interannual Variability in Phytoplankton Blooms Observed in the Northwestern Arabian Sea During the Southwest Monsoon, J. Geophys. Res., 97, 733–750, 1992.

Brock, J. C., McClain, C. R., Luther, M. E., and Hay, W. W.: The phytoplankton bloom in the northwestern Arabian Sea during the Southwest Monsoon of 1979, J. Geophys. Res., 96, 20623–20642, 1991.

Brodeau, L., Barnier, B., Penduff, T., Tréguier, A.-M., and Gulev, S.: An ERA40 based atmospheric forcing for global ocean circulation models, Ocean Model., 31, 88–104, doi:10.1016/j.ocemod.2009.10.005, 2009.

Chaigneaun, A., Eldin, G., and Dewitt, B.: Eddy activity in the four major upwelling systems from altimetry (1992–2007), Progr. Oceanogr., 83, 117–123, 2009.

Codispoti, L. A., Brandes, J. A., Christensen, J. P., Devol, A. H., Naqvi, S. W. A., Paerl, H. W., and Yoshinari, T.: The oceanic fixed nitrogen and nitrous oxide budgets: moving targets as we enter the anthropocene?, Sci. Mar., 65, 85–105, 2001.

de Sousa, S. N., Kumar, M. D., Sardessai, S., Sarma, V. V. S. S., and Shirodkar, P. V.: Seasonal variability in oxygen and nutrients in the central and eastern Arabian Sea, Curr. Sci., 71, 847–851, 1996.

Diaz, R. J. and Rosenberg, R.: Spreading dead zones and consequences for marine ecosystems., Science, 321, 26–29, 2008.

Dutkiewicz, S., Follows, M. J., and Parekh, P.: Interactions of the iron and phosphorus cycles: A three-dimensional model study, Global Biogeochem. Cy., 19, GB1021, doi:10.1029/2004GB002342, 2005.

Falkowski, P.: Evolution of the nitrogen cycle and its influence on the biological sequestration of CO_2 in the ocean, Nature, 327, 242–244, 1997.

Findlater, J.: A major low-level air current near the Indian Ocean during the northern summer, Q. J. R. Meteorol. Soc., 95, 362–380, 1969.

Fischer, A. S., Weller, R. A., Rudnick, D. L., Eriksen, C. C., Lee, C. M., Brink, K. H., Fox, C. A., and Leben, R. R.: Mesoscale eddies, coastal upwelling, and the upper-ocean heat budget in the Arabian Sea, Deep-Sea Res. Pt. II, 49, 2231–2264, doi:10.1016/S0967-0645(02)00036-X, the 1994–1996 Arabian Sea Expedition: Oceanic Response to Monsoonal Forcing, Part 5, 2002.

Flagg, C. and Kim, H.-S.: Upper ocean currents in the northern Arabian Sea from shipboard ADCP measurements during the 1994–1996 U.S. JGOFS and ONR programs, Deep-Sea Res. Pt. II, 45, 1917–1960, 1998.

Froelicher, T. L., Joos, F., Plattner, G.-K., Steinacher, M., and Doney, S. C.: Natural variability and anthropogenic trends in oceanic oxygen in a coupled carbon cycle–climate model ensemble, Global Biogeochem. Cy., 23, GB1003, doi:10.1029/2008GB003316, 2009.

Garrison, D. L., Gowing, M. M., and Hughes, M. P.: Nano- and microplankton in the northern Arabian Sea during the Southwest Monsoon, August–September 1995 A US-JGOFS study, Deep-Sea Res. Pt. II, 45, 2269–2299, doi:10.1016/S0967-0645(98)00071-X, 1998.

Gnanadesikan, A., Dunne, J. P., and John, J.: Understanding why the volume of suboxic waters does not increase over centuries of global warming in an Earth System Model, Biogeosciences, 9, 1159–1172, doi:10.5194/bg-9-1159-2012, 2012.

Han, W., McCreary, J. P., masumoto, Y., Vialard, J., and Duncan, B.: Basin modes in the equatorial Indian Ocean, J. Phys. Oceanogr., 41, 1252–1270, 2011.

Hitchcock, G. L., Key, E. L., and Masters, J.: The fate of upwelled waters in the Great Whirl, August 1995, Deep-Sea Res. Pt. II, 47, 1605–1621, doi:10.1016/S0967-0645(99)00156-3, 2000.

Honjo, S., Dymond, J., Prell, W., and Ittekkot, V.: Monsoon-controlled export fluxes to the interior of the Arabian Sea, Deep-Sea Res. Pt. II, 46, 1859–1902, doi:10.1016/S0967-0645(99)00047-8, 1999.

Kawamiya, M.: Mechanism of offshore nutrient supply in the western Arabian Sea, J. Mar. Res., 59, 675–696, 2001.

Keeling, R. F., Koertzinger, A., and Gruber, N.: Ocean Deoxygenation in a warming world, Annu. Rev. Mar. Sci., 2, 199–229, doi:10.1146/annurev.marine.010908.163855, 2010.

Keen, T., Kindle, J., and Young, D.: The interaction of Southwest Monsoon upwelling, advection and primary production in the northwest Arabian Sea, J. Mar. Syst., 13, 61–82, 1997.

Kim, H.-S., Flagg, C. N., and Howden, S.: Northern Arabian Sea variability from TOPEX/Poseidon altimetry data, An extension of the JGOFS/ONR shipboard ADCP study, Deep-Sea Res. Pt. II, 48, 1069–1096, 2001.

Klein, P., Hua, B. L., Lapeyre, G., Capet, X., Gentil, S. L., and Sasaki, H. S.: Upper ocean turbulence from high 3-d resolution simulations, J. Phys. Oceanogr., 38, 1748–1763, 2008.

Koné, V., Aumont, O., Lévy, M., and Resplandy, L.: Physical and Biogeochemical Controls of the Phytoplankton Seasonal Cycle in the Indian Ocean: a modeling study, in: Indian Ocean Biogeochemical Processes and Ecological Variability, edited by: Wiggert, J. D., Hood, R. R., Naqvi, S. W. A., Brink, K. H., and Smith, S. L., 185, 147–166, American Geophysical Union, Washington DC, USA, 2009.

Lam, P., Jensen, M. M., Kock, A., Lettmann, K. A., Plancherel, Y., Lavik, G., Bange, H. W., and Kuypers, M. M. M.: Origin and fate of the secondary nitrite maximum in the Arabian Sea, Biogeosciences, 8, 1565–1577, doi:10.5194/bg-8-1565-2011, 2011.

Lee, C. M., Jones, B. H., Brink, K. H., and Fischer, A. S.: The upper-ocean response to monsoonal forcing in the Arabian Sea: seasonal and spatial variability, Deep-Sea Res. Pt. II, 47, 1177–1226, 2000.

Levin, L. A., Ekau, W., Gooday, A. J., Jorissen, F., Middelburg, J. J., Naqvi, S. W. A., Neira, C., Rabalais, N. N., and Zhang, J.: Effects of natural and human-induced hypoxia on coastal benthos, Biogeosciences, 6, 2063–2098, doi:10.5194/bg-6-2063-2009, 2009.

Levitus, S., Boyer, T., Conkright, M., O'Brian, T., Antonov, J., Stephens, C., Stathopolos, L., Johnson, D., and Gelfeld, R.: World Ocean database 1998, Technical Report NESDID18, NOAA Atlas, 1998.

Lévy, M., Estubier, A., and Madec, G.: Choice of an advection scheme for biogeochemical models, Geophys. Res. Lett., 28, 3725–3728, 2001.

Lévy, M., Shankar, D., André, J.-M., Shenoi, S. S. C., Durand, F., and de Boyer Montégut, C.: Basin-wide seasonal evolution of the Indian Ocean's phytoplankton blooms, J. Geophys. Res., 112, C12014, doi:10.1029/2007JC004090, 2007.

Lévy, M., Klein, P., Tréguier, A.-M., Iovino, D., Madec, G., Masson, S., and Takahashi, K.: Modifications of gyre circulation by sub-mesoscale physics, Ocean Model., 34, 1–15, doi:10.1016/j.ocemod.2010.04.001, 2010.

Lierheimer, L. J. and Banse, K.: Seasonal and interannual variability of phytoplankton pigment in the Laccadive (Lakshadweep) Sea as observed by the Coastal Zone Color Scanner, P. Indian AS-Earth, 111, 163–185, 2002.

Madec, G.: NEMO, the ocean engine, Note du Pole de modelisation, Institut Pierre-Simon Laplace (IPSL), France, No 27 ISSN No 1288–1619, available at: www.nemo-ocean.eu/About-NEMO/Reference-manuals, 2008.

Madhupratap, S. P. K., Bhattathiri, P. M. A., Kumar, M. D., Raghukumar, S., Nair, K. K. C., and Ramaiah, N.: Mechanism of the biological response to winter cooling in the northern Arabian Sea, Nature, 384, 549–552, 1996.

Manghnani, V., Morrison, J. M., Hopkins, T. S., and Böhm, E.: Advection of upwelled waters in the form of plumes off Oman during the Southwest Monsoon, Deep-Sea Res. Pt. II, 45, 2027–2052, 1998.

Marchesiello, P., McWilliams, J. C., and Shchepetkin, A.: Equilibrium structure and dynamics of the California Current System, J. Phys. Oceanogr., 33, 753–783, 2004.

Marra, J., Dickey, T. D., Ho, C., Kinkade, C. S., Sigurdson, D. E., Weller, R. A., and Barber, R. T.: Variability in primary production as observed from moored sensors in the central Arabian Sea in 1995, Deep-Sea Res. Pt. II, 45, 2253–2267, doi:10.1016/S0967-0645(98)00070-8, 1998.

McCreary, J. P., Kundu, P. K., and Molinari, R. L.: A numerical investigation of dynamics, thermodynamics and mixed-layer processes in the Indian Ocean, Progr. Oceanogr., 31, 181–244, doi:10.1016/0079-6611(93)90002-U, 1993.

McCreary, J. P., Yu, Z., Hood, R., Vinaychandran, P. N., Furue, R., Ishida, A., and Richards, K.: Dynamics of the Indian-Ocean oxygen minimum zones, Progr. Oceanogr., accepted, 2012.

Moore, J. K., Doney, S. C., and Lindsay, K.: Upper ocean ecosystem dynamics and iron cycling in a global three-dimensional model, Global Biogeochem. Cy., 18, GB4028, doi:10.1029/2004GB002220, 2004.

Morrison, J. M., Codispoti, L. A., Smith, S. L., Wishner, K., Flagg, C., Gardner, W. D., Gaurin, S., Naqvi, S. W. A., Manghnani, V., Prosperie, L., and Gundersen, J. S.: The oxygen minimum zone in the Arabian Sea during 1995 - overall seasonal and geographic patterns, and relationship to oxygen gradients, Deep-Sea Res. Pt. II, 46, 1903–1931, doi:10.1016/S0967-0645(99)00048-X, 1999.

Naqvi, S. W. A., Yoshinari, T. Naik, H., Jayakumar, D. A., Altabet, M. A., Narvekar, P., Devol, A., Brandes, J. A., and Codispoti, L. A.: Budgetary and biogeochemical implications of N_2O isotope signatures in the Arabian Sea, Nature, 394, 462–464, 1998.

Naqvi, S. W. A., Naik, H., Pratihary, A., D'Souza, W., Narvekar, P. V., Jayakumar, D. A., Devol, A. H., Yoshinari, T., and Saino, T.: Coastal versus open-ocean denitrification in the Arabian Sea, Biogeosciences, 3, 621–633, doi:10.5194/bg-3-621-2006, 2006.

Nethery, D. and Shankar, D.: Vertical propagation of baroclinic Kelvin waves along the west coast of India, J. Earth Syst. Sc., 116, 331–339, 2007.

Olson, D. B., Hitchcock, G. L., Fine, R. A., and Warren, B. A.: Maintenance of the low-oxygen layer in the central Arabian Sea, Deep-Sea Res. Pt. II, 40, 673–685, doi:10.1016/0967-0645(93)90051-N, 1993.

Paulmier, A. and Ruiz-Pino, D.: Oxygen minimum zones (OMZs) in the modern ocean, Progr. Oceanogr., 80, 113–128, doi:10.1016/j.pocean.2008.08.001, 2009.

Prakash, S., Balakrishnan Nair, T. M., Udaya Bhaskar, T., Prakash, P., and Gilbert, D.: Oxycline variability in the central Arabian Sea: an Argo-oxygen study, J. Sea Res., 71, 1–8, 2012.

Rao, R., Molinari, R., and Festa, J.: Evolution of the Climatological Near-Surface Thermal Structure of the Tropical Indian Ocean 1. Description of Mean Monthly Mixed Layer Depth, and Sea Surface Temperature, Surface Current, and Surface Meteorological Fields, J. Geophys. Res., 94, 10801–10815, 1989.

Resplandy, L., Lévy, M., Madec, G., Pous, S., Aumont, O., and Kumar, D.: Contribution of mesoscale processes to nutrient budgets in the Arabian Sea, J. Geophys. Res., 116, C11007, doi:10.1029/2011JC007006, 2011.

Ryther, J. H. and Menzel, D. W.: On the production, composition, and distribution of organic matter in the Western Arabian Sea, Deep-Sea Res. Pt. I, 12, 199–209, 1965.

Sarma, V. V. S. S.: An evaluation of physical and biogeochemical processes regulating perennial suboxic conditions in the water column of the Arabian Sea, Global Biogeochem. Cy., 16, 1082, doi:10.1029/2001GB001461, 2002.

Sarmiento, J. L., Hughes, T. M. C., Stouffer, R. J., and Manabe, S.: Simulated response of the ocean carbon cycle to anthropogenic climate warming, Nature, 393, 245–249, 1998.

Schott, F. A. and McCreary, J. P.: The monsoon circulation of the Indian Ocean, Progr. Oceanogr., 51, 1–123, 2001.

Shchepetkin, A. F. and McWilliams, J. C.: The regional oceanic modeling system (ROMS): a split-explicit, free-surface, topography-following-coordinate oceanic model, Ocean Model., 9, 347–404, doi:10.1016/j.ocemod.2004.08.002, 2005.

Shetye, S. R., Gouveia, A. D., Shenoi, S. S. C., Sundar, D., Michael, G. S., Almeida, A. M., and Santanam, K.: Hydrography and circulation off the West coast of India during the Southwest monsoon 1987, J. Mar. Res., 48, 359–378, 1990.

Stramma, L., Johnson, G. C., Sprintall, J., and Mohrholz, V.: Expanding Oxygen-Minimum Zones in the Tropical Oceans, Science, 320, 655–658, doi:10.1126/science.1153847, 2008.

Stramma, L., Prince, E. D., Schmidtko, S., Luo, J., Hoolihan, J. P., Visbeck, M., Wallace, D. W. R., Brandt, P., and Koertzinger, A.: Expansion of oxygen minimum zones may reduce available habitat for tropical pelagic fishes, Nat. Clim. Change, 2, 33–37, doi:10.1038/nclimate1304, 2011.

Stramma, L., Oschlies, A., and Schmidtko, S.: Mismatch between observed and modeled trends in dissolved upper-ocean oxygen over the last 50 yr, Biogeosciences, 9, 4045–4057, doi:10.5194/bg-9-4045-2012, 2012.

Sverdrup, H., U., Johnson, M. W., and Fleming, R. H.: The Ocean: Their Physics, Chemistry and General Biology, Prentice-Hall, p. 696, old Tappan, 1942.

Swallow, J., C.: Some aspects of the physical oceanography of the Indian Ocean, Deep-Sea Res., 31, 639–650, 1984.

Takahashi, T., Broecker, W. S., and Langer, S.: Redfield ratio based on chemical data from isopycnal surfaces, J. Geophys. Res., 90, 6907–6924, 1985.

Treguier, A., Barnier, B., de Miranda, A., Molines, J. M., Grima, N., Imbard, M., Madec, G., Messager, C., Reynaud, T., and Michel, S.: An eddy-permitting model of the Atlantic circulation: Evaluating open boundary conditions, J. Geophys. Res., 106, 22115–22129, 2001.

Van Leer, B.: Towards the Ultimate Conservative Difference Scheme, V. a Second Order Sequel to Godunov's Method, J. Comput. Phys., 32, 101–136, 1979.

Veldhuis, M. J. W., Kraay, G. W., Bleijswijk, J. D. L. V., and Baars, M. A.: Seasonal and spatial variability in phytoplankton biomass, productivity and growth in the northwestern Indian Ocean: the Southwest and Northeast Monsoon, 1992-1993, Deep-Sea Res. Pt. I, 44, 425–449, doi:10.1016/S0967-0637(96)00116-1, 1997.

Weller, R. A., Fischer, A. S., Rudnick, D. L., Eriksen, C. C., Dickey, T. D., Marra, J., Fox, C., and Leben, R.: Moored observations of upper-ocean response to the monsoons in the Arabian Sea during 1994–1995, Deep-Sea Res. Pt. II, 49, 2195–2230, doi:10.1016/S0967-0645(02)00035-8, the 1994–1996 Arabian Sea Expedition: Oceanic Response to Monsoon al Forcing, Part 5, 2002.

Wiggert, J. D. and Murtugudde, R. G.: The sensitivity of the southwest monsoon phytoplankton bloom to variations in aeolian iron deposition over the Arabian Sea, J. Geophys. Res., 112, C05005, doi:10.1029/2006JC003514, 2007.

Wiggert, J. D., Hood, R., Banse, K., and Kindle, J.: Monsoon-driven biogeochemical processes in the Arabian Sea, Progr. Oceanogr., 65, 176–213, doi:10.1016/j.pocean.2005.03.008, the Arabian Sea of the 1990s: New Biogeochemical Understanding, 2005.